Journal of Advanced Ceramics
2015, **4**(4): 253–259
DOI: 10.1007/s40145-015-0157-x

ISSN 2226-4108
CN 10-1154/TQ

Research Article

Thermophysical properties of uranium–europium mixed oxides

R. VENKATA KRISHNAN, R. BABU, Abhiram SENAPATI,
G. JOGESWARARAO, K. ANANTHASIVAN*

Fuel Chemistry Division, Indira Gandhi Centre for Atomic Research, Kalpakkam-603102, Tamil Nadu, India

Received: April 16, 2015; Revised: May 12, 2015; Accepted: May 18, 2015

Abstract: Uranium–europium mixed oxides $(U_{1-y}Eu_y)O_{2-x}$ ($y=0.2$–0.8) were prepared by the citrate gel combustion technique and characterized by X-ray diffraction (XRD). Single phase fluorite structure was observed in those solid solutions with $y\leqslant 0.6$. The solid solutions with $y>0.6$ were found to be biphasic, with the second phase being cubic Eu_2O_3. Heat capacity and enthalpy increment measurements were carried out by using differential scanning calorimeter (DSC) and drop calorimeter in the temperature range 298–800 K and 800–1800 K, respectively. The $C_{p,m}$ values at 298 K for $(U_{1-y}Eu_y)O_{2-x}$ ($y=0.2$, 0.4, 0.6) are 64.8, 64.6, and 63.5 $J\cdot K^{-1}\cdot mol^{-1}$, respectively. An anomalous increase was observed in the heat capacity in all of the solid solutions with the onset temperature around 950 K. This could be attributed to the contribution from Frenkel pair oxygen defects. From the excess heat capacity data, the enthalpy for the formation of these defects was computed and found to be in the range of 2.10±0.02 eV.

Keywords: uranium; europium; solid solution; calorimetry; heat capacity; Frenkel defects

1 Introduction

Solid solution of uranium–plutonium mixed oxides is used as a driver fuel in fast reactors. Fission products formed during the irradiation of the fuel are found within its matrix as metallic inclusions, oxide precipitates, and oxide solid solutions. Hence, the composition and the physiochemical properties of the fuel get significantly altered [1–3]. Thermal induced transport phenomena and chemical interactions among these constituents further accelerate the changes. The thermal conductivity and heat capacity of these solid solutions are important to understand the in-pile behaviour of the fuel. Among the fission products, the rare earths form a sizable fraction (fission yield 50 at%) [4]. Owing to their ionic radii (in their oxides) that are comparable with those of fuel constituents (U and Pu), the rare earths are significantly soluble in the mixed oxide fuel matrix [5]. The studies on the solid solubility of $EuO_{1.5}$ in UO_2, oxygen potentials of uranium–europium solid solutions, as well as their defect chemistry, have been reported in the literature [5–9]. Heat capacity data on uranium–europium mixed oxides with europium content of 4.4 and 9.0 mol% have been reported by Matsui *et al.* [10]. These authors have observed anomalous increase in the heat capacity, which sets in at temperatures ranging from 950 to 1150 K. Such an anomalous increase in the heat capacity observed in UO_2 doped with rare earth oxides ($REO_{1.5}$, RE = La, Gd, Nd) has been reported in our earlier works [11–13]. Matsui *et al.* [10] reported the heat capacity measured by using direct heating pulse calorimetry in the temperature range 300–1550 K for

---

* Corresponding author.
E-mail: asivan@igcar.gov.in

$(U_{1-y}Eu_y)O_{2-x}$ ($y = 0.044$–0.09). In the present work, the heat capacity and enthalpy increment measurements of $(U_{1-y}Eu_y)O_{2-x}$ were carried out over a wide range of composition ($y = 0.2$–0.8). These results are discussed in this paper.

2 Experimental

2. 1 Sample preparation and characterization

Europium oxide of 99.99% purity supplied by M/s. Indian Rare Earths and nuclear grade uranium oxide supplied by NFC, Hyderabad, were used for preparing the samples. The solid solutions $(U_{1-y}Eu_y)O_{2-x}$ ($y = 0.2$–0.8) were prepared by citrate gel combustion synthesis. The procedure using which these samples were prepared was reported in our earlier publication [12]. These sample pellets were reduced by heating them in a stream of Ar+8%H_2 gas mixture at 873 K. Subsequently these pellets were sintered at 1873 K for 6 h. A heating/cooling rate was maintained 200 $K\cdot h^{-1}$. Before heating the samples, the furnace was evacuated (10^{-3} mbar) and filled with ultra high pure Ar+8%H_2 gas mixture thrice. The concentrations of U and Eu in the sintered sample pellets were determined by inductively coupled plasma atomic emission spectroscopy (ICP-AES). The concentrations of other metallic impurities were determined by inductively coupled plasma mass spectrometer (ICP-MS) (model number ELAN 250 of M/s. Perkn Helmer, Canada). The samples were analyzed for carbon impurity by using carbon analyzer (model number ELTRACS 800 of M/s. Eltra, Germany). Structural characterization was carried out by using X-ray diffraction (XRD). The XRD patterns were recorded in the range $10° < 2\theta < 80°$. Peak positions and their relative intensities were computed by using a peak-fit program, which was part of the Philips X'pert Plus® software. The calibration of the diffractometer was carried out by using single crystal silicon and α-alumina standards. The lattice parameter pertaining to the solid solution samples was estimated from the 2θ values pertaining to eight major reflections of the oxide with CaF_2 structure. Finally an effective high angle corrected lattice parameter at each temperature was obtained by the standard Nelson Riley extrapolation procedure.

2. 2 Calorimetric measurements

A heat flux type differential scanning calorimeter (DSC, model number DSC821e/700 of M/s. Mettler Toledo GmbH, Switzerland) was used in this study. Temperature, heat flow, heat flow rate, and τ-lag calibrations were carried out, as explained in our previous publications [11,14,15]. The uncertainty in the heat capacity data measured by the DSC was estimated to be about 2%–3% based on our previous measurements on standard ThO_2 samples [15]. The enthalpy increments of these samples in the temperature range 800–1800 K were determined by using a high temperature drop calorimeter equipped with multi-detector (MHTC-96) supplied by M/s. SETARAM. The procedures used in the measurement of heat capacity and enthalpy increment are described elsewhere [11–15].

3 Results and discussion

3. 1 Chemical assay and phase characterization

The results of the impurity analysis carried out by using ICP-MS and carbon analyzer are listed in Table 1. The total concentration of impurities in all these solid solutions is found to be less than 500 ppm. The results of the chemical assay (concentrations of U and Eu) by ICP-AES shown in Table 2 are in good agreement within ±1% of the expected values. The room temperature XRD patterns pertaining to $(U_{1-y}Eu_y)O_{2-x}$ ($y = 0.2$–0.8) are shown in Fig. 1. It is evident from this figure that the solid solutions $(U_{1-y}Eu_y)O_{2-x}$ ($y = 0.2$–0.65) show a single phase fluorite structure, whereas in the XRD patterns pertaining to samples with y values greater than 0.65, additional peaks pertaining to the cubic Eu_2O_3 phase [16] are observed. However, scanning electron microscopy–energy dispersive X-ray analysis (SEM–EDAX) of $(U_{0.35}Eu_{0.65})O_{2-x}$ confirms the precipitation of the cubic Eu_2O_3 phase. The results of the EDAX analysis of $(U_{1-y}Eu_y)O_{2-x}$ ($y = 0.2, 0.4, 0.6, 0.65$) are shown in Fig. 2. In the SEM analysis of the solid solutions, $(U_{1-y}Eu_y)O_{2-x}$ pertaining up to the value of y equal to 0.6, only cuboidal (plate) like microstructures are formed. However, for $(U_{0.35}Eu_{0.65})O_{2-x}$ in addition to cuboidal crystallites, acicular (rod) like microstructures are also found. EDAX analysis on various positions of the pellets of $(U_{1-y}Eu_y)O_{2-x}$ ($y = 0.2$, 0.4, 0.6) shows uniform composition pertaining to that of solid solution confirming the phase homogeneity throughout the pellet. However, for $(U_{0.35}Eu_{0.65})O_{2-x}$, the EDAX analysis (Fig.

Table 1 Concentrations of impurities in U–Eu mixed oxides using ICP-MS

Element	Concentration of impurity (ppm)		
	$(U_{0.8}Eu_{0.2})O_{2-x}$	$(U_{0.6}Eu_{0.4})O_{2-x}$	$(U_{0.4}Eu_{0.6})O_{2-x}$
Ni	10	9	5
Zn	5	6	3
Mo	14	10	7
Ba	<1	<1	<1
Al	<1	<1	2
Mg	<1	<1	<1
Ca	<1	8	3
V	<1	<1	<1
Cr	16	9	8
Mn	6	1	2
Fe	56	45	54
Cu	<1	<1	2
Ce	14	4	8
La	<1	6	14
Sm	<1	<1	1
Nd	<1	<1	<1
Gd	18	28	31
Dy	<1	<1	<1
C	<100	<100	<100

Table 2 Relative concentrations of U and Eu determined by ICP-AES

Solid solution	U (mol%)	Eu (mol%)
$(U_{0.8}Eu_{0.2})O_{2-x}$	79.9	20.1
$(U_{0.6}Eu_{0.4})O_{2-x}$	60.2	39.8
$(U_{0.4}Eu_{0.6})O_{2-x}$	39.9	60.1
$(U_{0.35}Eu_{0.65})O_{2-x}$	35.2	64.8
$(U_{0.3}Eu_{0.7})O_{2-x}$	30.1	69.9
$(U_{0.25}Eu_{0.75})O_{2-x}$	24.9	75.1
$(U_{0.2}Eu_{0.8})O_{2-x}$	19.9	80.1

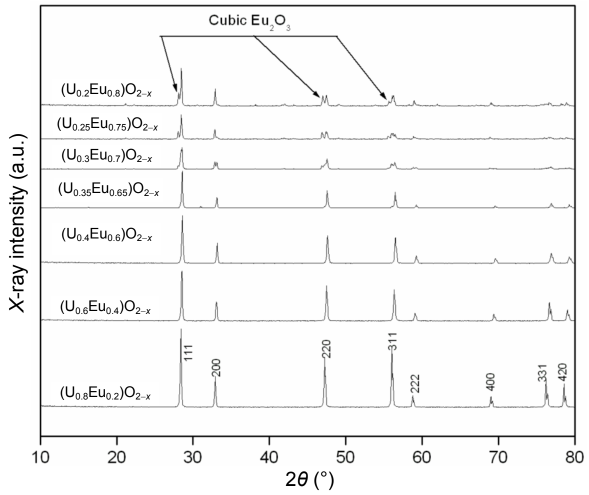

Fig. 1 Room temperature XRD patterns of $(U_{1-y}Eu_y)O_{2-x}$ ($y = 0.2$–0.8).

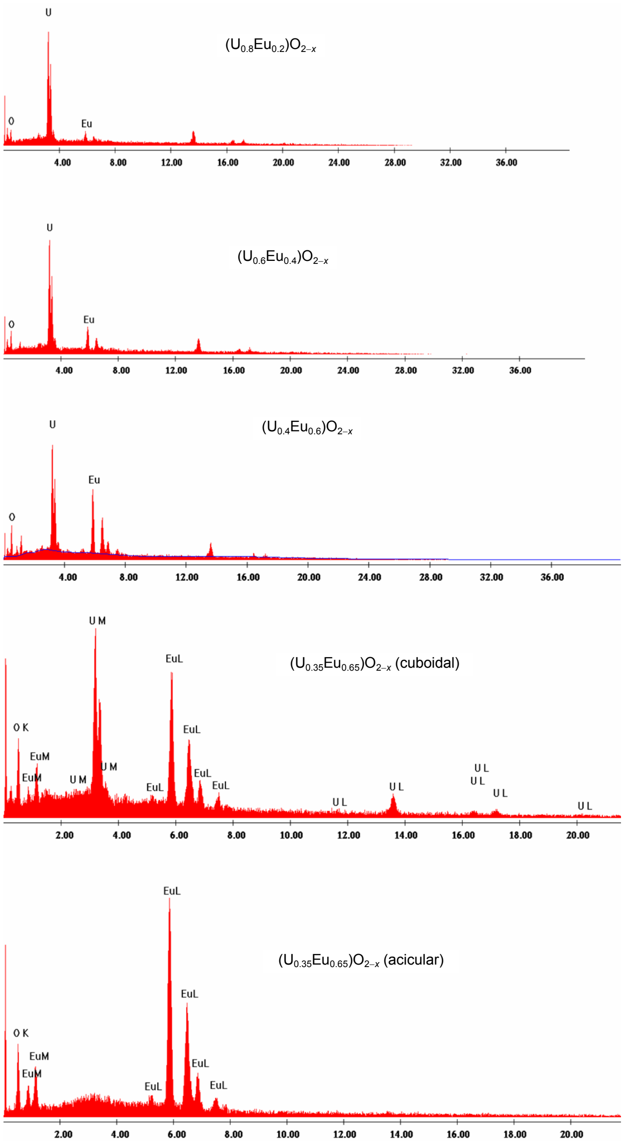

Fig. 2 Results of EDAX analysis of $(U_{1-y}Eu_y)O_{2-x}$ ($y = 0.2$, 0.4, 0.6, 0.65).

2) on cuboidal crystallites shows peaks pertaining to U, Eu, and O (composition pertaining to solid solution), whereas that on acicular crystallites shows peaks pertaining to only Eu and O. The lattice parameter of $(U_{1-y}Eu_y)O_{2-x}$ ($y = 0.2$, 0.4, 0.6) decreases with the Eu content of the solid solution and the values of lattice parameters are 0.5451, 0.5437, and 0.5425 nm, respectively. Upon increasing the concentration of Eu in these solid solutions, no change is observed in their lattice parameters. Therefore, it is evident that the terminal solid solubility of $EuO_{1.5}$ in UO_2 is in the range of 60–65 mol%. The heat capacity and enthalpy increment measurements were carried out only on the single phase solid solutions $(U_{1-y}Eu_y)O_{2-x}$ ($y = 0.2$, 0.4, 0.6).

3.2 Calorimetric measurements

The measured values of the enthalpy increment in the temperature range 800–1800 K were fitted into a four-term polynomial function represented below (by least squares regression analysis):

$$H_T - H_{298} = AT + B\times10^{-3}T^2 + C\times10^5T^{-1} + D\times10^4 \tag{1}$$

where A, B, and C are the coefficients obtained from the polynomial fit. The constraints used for this fit are (i) $H_T - H_{298} = 0$ at 298 K and (ii) the temperature derivative of the function at 298 K is equal to $C_{p,298}$ (measured by using DSC). The coefficients of those polynomials pertaining to the solid solutions $(U_{1-y}Eu_y)O_{2-x}$ ($y = 0.2, 0.4, 0.6$) are presented in Table 3. The plot of temperature dependence of the enthalpy increment corresponding to $(U_{1-y}Eu_y)O_{2-x}$ ($y = 0.2$, 0.4, 0.6) are presented in Fig. 3.

The values of the heat capacity measured by using DSC and those computed from the enthalpy increment by using drop calorimeter were fitted into a polynomial through a least squares regression analysis. The expressions for the temperature dependence of heat capacity values corresponding to the solid solutions $(U_{1-y}Eu_y)O_{2-x}$ ($y = 0.2, 0.4, 0.6$) are presented in Table 4. From these heat capacity data, the enthalpy, entropy, and Gibbs energy functions were computed. These results are presented in Tables 5–7. The values of S_{298} pertaining to $(U_{1-y}Eu_y)O_{2-x}$, required for the computation of S_T were estimated by using Neumann-Kopp's approximation by using the values of S^0_{298} of Eu_2O_3 [17] and UO_2 [18].

The combined fit of the heat capacity of $(U_{1-y}Eu_y)O_{2-x}$ ($y = 0.2$, 0.4, 0.6) obtained from the DSC and drop calorimetric experiments is shown in Fig. 4. As seen in the figure, the heat capacity values of $(U_{1-y}Eu_y)O_{2-x}$ ($y =$ 0.2, 0.4, 0.6) decrease with an increase in the Eu content of the solid solution. The dependence of phonon frequencies on the reduced mass of an oscillator comprising masses m_1 and m_2 is given in Eqs. (2) and (3).

Table 3 Coefficients in the function obtained by least squares regression analysis (800 K ≤ T ≤ 1800 K) for $(U_{1-y}Eu_y)O_{2-x}$

Coefficient	$(U_{0.8}Eu_{0.2})O_{2-x}$	$(U_{0.6}Eu_{0.4})O_{2-x}$	$(U_{0.4}Eu_{0.6})O_{2-x}$
A	80.1	77.9	75.5
B	1.35	1.34	1.63
C	1.39	1.20	1.10
D	−2.87	−2.74	−2.64
Standard error (J·mol^{-1})	14	15	80

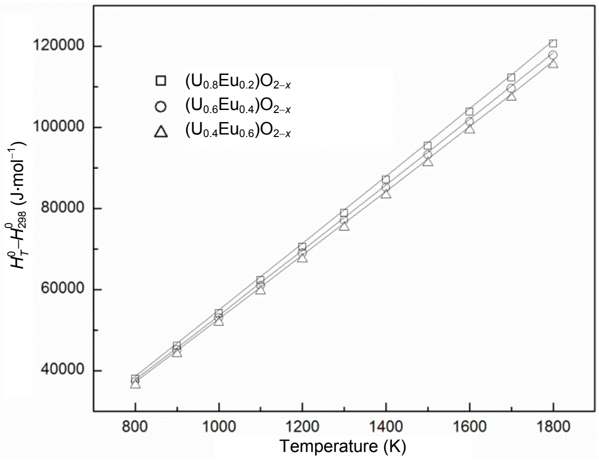

Fig. 3 Enthalpy increment of $(U_{1-y}Eu_y)O_{2-x}$ from drop calorimetry.

Table 4 Expressions obtained by least squares regression analysis for the temperature dependence of heat capacity (298 K ≤ T ≤ 1800 K) for $(U_{1-y}Eu_y)O_{2-x}$

Compound	Fit equation (J·K^{-1}·mol^{-1})	Standard error (J·K^{-1}·mol^{-1})
$(U_{0.8}Eu_{0.2})O_{2-x}$	$87.51–6.79\times10^{-3}T–1.877632\times10^6T^{-2} + 3.0739\times10^{-6}T^2$	1.02
$(U_{0.6}Eu_{0.4})O_{2-x}$	$84.40–5.84\times10^{-3}T–1.631278\times10^6T^{-2} + 2.7889\times10^{-6}T^2$	0.84
$(U_{0.4}Eu_{0.6})O_{2-x}$	$85.00–9.39\times10^{-3}T–1.696035\times10^6T^{-2} + 4.226\times10^{-6}T^2$	1.09

Table 5 Thermodynamic functions pertaining to $(U_{0.8}Eu_{0.2})O_{2-x}$

T (K)	$C_{p,m}$(J·K^{-1}·mol^{-1})		H_T-H_{298}(J·mol^{-1})		S_T	G_T-H_{298}/T
	Measured	Fit	Measured	Fit	(J·K^{-1}·mol^{-1})	(J·K^{-1}·mol^{-1})
298	64.77	64.62		0	88.9	−88.9
300	65.02	64.89		130	89.3	−88.9
400	73.24	73.55		7116	109.4	−91.6
500	77.48	77.37		14685	126.2	−96.9
600	80.16	79.33		22530	140.5	−103.0
700	82.09	80.43		30523	152.9	−109.2
800	83.64	81.11	38029	38602	163.6	−115.4
900		81.57	46078	46738	173.2	−121.3
1000		81.92	54192	54913	181.8	−126.9
1100		82.21	62361	63119	189.7	−132.3
1200		82.48	70578	71354	196.8	−137.4
1300		82.77	78838	79616	203.4	−142.2
1400		83.07	87138	87908	209.6	−146.8
1500		83.41	95475	96231	215.3	−151.2
1600		83.78	103847	104590	220.7	−155.3
1700		84.20	112253	112989	225.8	−159.3
1800		84.67	120691	121432	230.6	−163.2

Table 6 Thermodynamic functions pertaining to $(U_{0.6}Eu_{0.4})O_{2-x}$

T (K)	$C_{p,m}$ ($J\cdot K^{-1}\cdot mol^{-1}$) Measured	Fit	H_T-H_{298} ($J\cdot mol^{-1}$) Measured	Fit	S_T ($J\cdot K^{-1}\cdot mol^{-1}$)	G_T-H_{298}/T ($J\cdot K^{-1}\cdot mol^{-1}$)
298	64.64	64.54		0	81.7	−81.7
300	64.85	64.78		129	82.1	−81.7
400	72.12	72.32		7040	102.0	−84.4
500	75.81	75.65		14459	118.5	−89.6
600	78.10	77.37		22119	132.5	−95.6
700	79.72	78.35		29909	144.5	−101.8
800	80.99	78.97	37281	37777	155.0	−107.8
900		79.39	45126	45696	164.3	−113.5
1000		79.72	53032	53652	172.7	−119.0
1100		80.01	60988	61639	180.3	−124.3
1200		80.28	68989	69653	187.3	−129.2
1300		80.56	77031	77695	193.7	−134.0
1400		80.86	85111	85765	199.7	−138.4
1500		81.19	93226	93868	205.3	−142.7
1600		81.56	101375	102005	210.5	−146.8
1700		81.97	109557	110181	215.5	−150.7
1800		82.42	117770	118401	220.2	−154.4

Table 7 Thermodynamic functions pertaining to $(U_{0.4}Eu_{0.6})O_{2-x}$

T (K)	$C_{p,m}$ ($J\cdot K^{-1}\cdot mol^{-1}$) Measured	Fit	H_T-H_{298} ($J\cdot mol^{-1}$) Measured	Fit	S_T ($J\cdot K^{-1}\cdot mol^{-1}$)	G_T-H_{298}/T ($J\cdot K^{-1}\cdot mol^{-1}$)
298	63.48	63.48		0	76.0	−76.0
300	63.70	63.72		127	76.4	−76.0
400	71.25	71.32		6937	95.9	−78.6
500	74.99	74.57		14252	112.2	−83.7
600	77.23	76.17		21798	126.0	−89.7
700	78.77	77.03		29462	137.8	−95.7
800	79.93	77.54	36467	37193	148.1	−101.6
900		77.87	44140	44965	157.3	−107.3
1000		78.14	51877	52766	165.5	−112.7
1100		78.38	59668	60591	173.0	−117.9
1200		78.64	67509	68442	179.8	−122.8
1300		78.93	75395	76320	186.1	−127.4
1400		79.27	83324	84229	192.0	−131.8
1500		79.67	91294	92176	197.4	−136.0
1600		80.13	99302	100165	202.6	−140.0
1700		80.66	107349	108204	207.5	−143.8
1800		81.26	115432	116299	212.1	−147.5

$$\upsilon = \frac{1}{2\pi}(k/\mu) \quad (2)$$

$$\mu = \frac{m_1 \cdot m_2}{m_1 + m_2} \quad (3)$$

where υ is the phonon frequency; k is the force constant; and μ is the reduced mass. The atomic weight of U is 238.03 while that of Eu is 151.97. Doping of Eu in UO_2 lattice will lead to a decrease in the reduced mass. The lower the reduced mass, the higher would be the phonon frequency. The higher the phonon frequency, the lower would be the heat capacity. The increase in the phonon frequency due to the above mentioned factor contributes to the decrease in the heat capacity of $(U_{1-y}Eu_y)O_{2-x}$ with an increase in the concentration of Eu.

From Fig. 4, it is evident that considerable anomalous increase in the heat capacity is found to set in at onset temperatures ranging from 950 to 1000 K in all these solid solutions. Such anomalous increase in the heat capacity is usually observed when UO_2 is doped with an aliovalent cation (in this case Eu^{+3}, Eu^{+2}). This phenomenon was reported earlier [11–13,19–25] and has been ascribed to the formation of oxygen Frenkel defect pairs. An estimate of the temperature dependence of the heat capacity pertaining to the solid solutions $(U_{1-y}Eu_y)O_{2-x}$ ($y=0.2$, 0.4, 0.6) over the temperature range 298–1800 K was obtained by extrapolating the expression derived through the least squares regression analysis of these data in the temperature range 298–900 K. This would hence forth be termed as baseline heat capacity. The baseline (298–900 K) and the combined experimentally determined temperature dependence of heat capacity data in the temperature range 298–1800 K were fitted to the following polynomials by least squares regression analysis, respectively:

$$C_p(\text{baseline}) = A + BT + CT^{-2} \quad (4)$$

$$C_p(\text{experimental}) = A + BT + CT^{-2} + DT^2 \quad (5)$$

The temperature dependence of the heat capacity values (baseline and combined experimental values) is shown in Fig. 4. The difference between these values of the heat capacity is termed as the excess heat capacity (ΔC_p) [10–13]. The temperature dependence of this

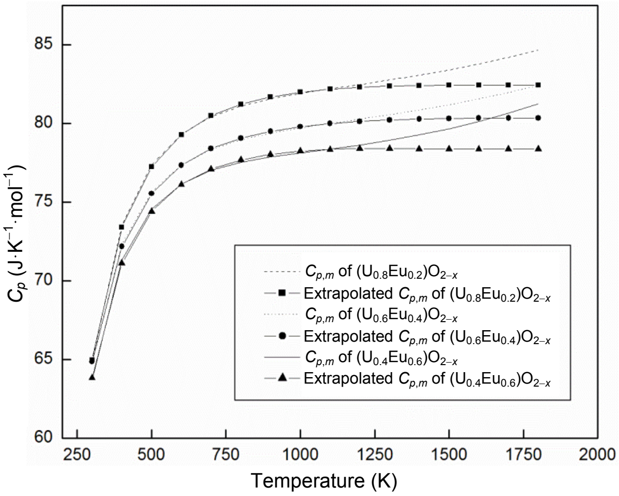

Fig. 4 Temperature dependent heat capacity data of $(U_{1-y}Eu_y)O_{2-x}$ ($y=0.2$, 0.4, 0.6).

excess heat capacity is shown in Fig. 5. It is evident from this figure that the onset temperature of heat capacity anomaly is around 950 K for all of the solid solutions $(U_{1-y}Eu_y)O_{2-x}$. Matsui *et al.* [10] measured the heat capacities of $(U_{1-y}Eu_y)O_2$ ($y = 0.044$–0.09) and have observed that the temperature at which the anomalous increase in the heat capacity sets in gets lowered with an increase in the concentration of Eu in the solid solution. These authors attributed this phenomenon to the decrease in the enthalpy of the formation of defects (ΔH_d) with an increase in the dopant concentration. However, it is seen in our earlier work on $(U_{1-y}Gd_y)O_{2\pm x}$ [13] and $(U_{1-y}La_y)O_{2\pm x}$ [11] that the onset temperature of the heat capacity anomaly as well as the enthalpy for the formation of defects do not decrease continuously with increase in the dopant (aliovalent cation) concentration. The onset temperature of heat capacity anomaly decreases with increase in dopant concentration and then reaches a plateau. The concentration of dopant over which there will not be any decrease in the enthalpy and defect formation and the onset temperature of heat capacity anomaly is a function of the nature of the dopant. In the case of $(U_{1-y}Gd_y)O_{2\pm x}$ and $(U_{1-y}La_y)O_{2\pm x}$, it lies in the range of 15–20 mol% $GdO_{1.5}$ and 20–40 mol% $LaO_{1.5}$, respectively [11,13].

The excess heat capacity (ΔC_p) due to the formation of Frenkel pair defects of oxygen is given by the following expression [10]:

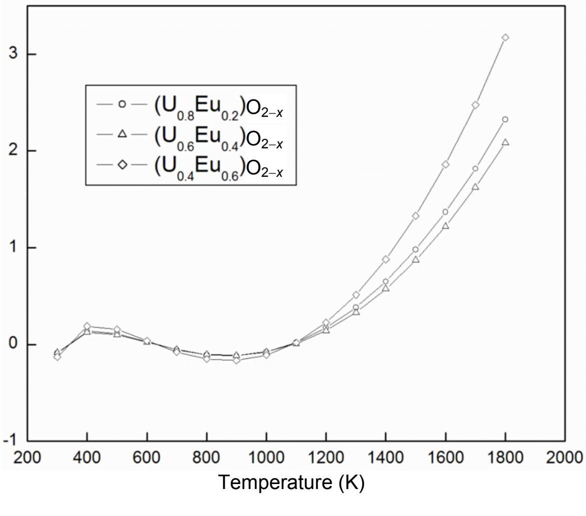

Fig. 5 Variation in the difference between the baseline and measured values of heat capacity (ΔC_p) with temperature of $(U_{1-y}Eu_y)O_{2-x}$ ($y = 0.2$, 0.4, 0.6).

$$\Delta C_p = \frac{(\Delta H_\mathrm{d})^2}{\sqrt{2}RT^2}\exp(\Delta S_\mathrm{d}/2R)\exp(-\Delta H_\mathrm{d}/2RT) \qquad (6)$$

where R is the gas constant; ΔH_d and ΔS_d are the enthalpy and entropy for the formation of Frenkel pair defects of oxygen, respectively. The plot of $\ln(\Delta C_p T^2)$ against $1/T$ is a straight line with a slope of $-\Delta H_\mathrm{d}/2R$. This plot for $(U_{1-y}Eu_y)O_{2-x}$ ($y = 0.2$, 0.4, 0.6) is shown in Fig. 6, and the enthalpy of defect formation computed from the slopes for all the solid solutions remains the same (2.10±0.02 eV). The value of ΔH_d reported by Matsui *et al.* [10] for $(U_{1-y}Eu_y)O_2$ ($y = 0.09$) is 1.7±0.2 eV. Therefore, it can be ascertained that there is no further decrease in the enthalpy of defect formation when the concentration of Eu increases from $y = 0.09$ to $y = 0.2$. The slight increase in the enthalpy of the defect formation observed from the present measurement may be due to errors in fitting. Therefore, the plateau region of the concentration of $EuO_{1.5}$ over which there will not be any decrease in the enthalpy of the defect formation may be in the values between 9 and 20 mol% $EuO_{1.5}$.

4 Conclusions

Heat capacity and enthalpy increment data pertaining $(U_{1-y}Eu_y)O_{2-x}$ over the extensive range of composition (20–60 mol% Eu) are reported for the first time. The heat capacity of these solid solution decreases with the Eu content at all temperatures. An anomalous increase in the heat capacity is observed with the onset temperature around 950 K and is attributed to the

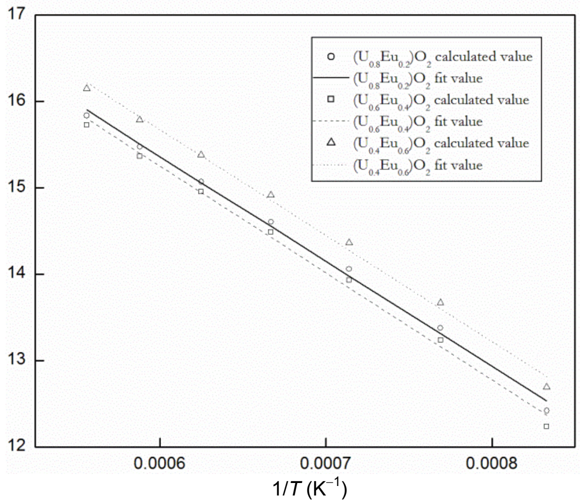

Fig. 6 Plot of $\ln(\Delta C_p T^2)$ vs. $1/T$ in the temperature range 900–1800 K.

formation oxygen Frenkel defect pairs. The enthalpy for the formation of these defects is computed from the excess heat capacity and is found to be nearly the same for all the solid solutions (2.10±0.02 eV).

References

[1] Olander DR. *Fundamental Aspects of Nuclear Reactor Fuel Elements*. Virgina, USA: Springfield, 1985.

[2] Matzke Hj. *Science of Advanced LMFBR Fuels*. Amsterdam: Elsevier, 1986.

[3] IAEA-TECDOC-1168. Compilation and evaluation of fission yield nuclear data. 2000. Available at http://www-pub.iaea.org/MTCD/Publications/PDF/te_1168_prn.pdf.

[4] Crouch EAC. Calculated independent yields in thermal neutron fission of sup233U, sup235U, sup239Pu, sup241Pu, and in fission of sup232Th, sup238U, and sup240Pu. Technical Report AERE-R-6056. 1969.

[5] Grossman LN, Lewis JE, Rooney DM. The system UO_2–Eu_2O_3 at high temperatures. *J Nucl Mater* 1967, **21**: 302–309.

[6] Fujino T, Ouchi K, Mozumi Y, *et al*. Composition and oxygen potential of cubic fluorite-type solid solution $Eu_yU_{1-y}O_{2+x}$ ($x \equiv 0$) and rhombohedral $Eu_6UO_{12+x'}$ ($x' < 0$). *J Nucl Mater* 1990, **174**: 92–101.

[7] Haug H, Weigel F. Mischoxidsysteme von lanthaniden- und actinidenelementen: I. Röntgen-untersuchungen im system Uranoxid-Europiumoxid. *J Nucl Mater* 1963, **9**: 355–359.

[8] Omichi T, Fukushima S, Maeda A, *et al*. On the relation between lattice parameters and O/M ratio for uranium dioxide–trivalent rare earth oxide solid solution. *J Nucl Mater* 1981, **102**: 40–46.

[9] Park K, Olander DR. Defect models for the oxygen potentials of gadolinium- and europium-doped urania. *J Nucl Mater* 1992, **187**: 89–96.

[10] Matsui T, Kawase T, Naito K. Heat capacities and electrical conductivities of $(U_{1-y}Eu_y)O_2$ ($y = 0.044$ and 0.090) from 300 to 1550 K. *J Nucl Mater* 1992, **186**: 254–258.

[11] Venkata Krishnan R, Mittal VK, Babu R, *et al*. Heat capacity measurements and XPS studies on uranium–lanthanum mixed oxides. *J Alloys Compd* 2011, **509**: 3229–3237.

[12] Venkata Krishnan R, Babu R, Panneerselvam G, *et al*. Solubility studies and thermophysical properties of uranium–neodymium mixed oxides system. *Ceram Int* 2014, **40**: 4395–4405.

[13] Venkata Krishnan R, Panneerselvam G, Manikandan P, *et al*. Heat capacity and thermal expansion of uranium–gadolinium mixed oxides. *J Nucl Radiochem Sci* 2009, **10**: 19–26.

[14] Venkata Krishnan R, Nagarajan K, Vasudeva Rao PR. Heat capacity measurements on $BaThO_3$ and $BaCeO_3$. *J Nucl Mater* 2001, **299**: 29–31.

[15] Venkata Krishnan R, Nagarajan K. Heat capacity measurements on uranium–cerium mixed oxides by differential scanning calorimetry. *Thermochim Acta* 2006, **440**: 141–145.

[16] International Centre for Diffraction Data. Powder diffraction files (inorganic phases). Joint Committee on Powder Diffraction Data (JCPDS), ICDD card number 00-034-0392. 2013.

[17] Knacke O, Kubaschewski O, Hesselmann K. *Thermochemical Properties on Inorganic Substances*. Berlin: Springer, 1991.

[18] Fink JK. Thermophysical properties of uranium dioxide. *J Nucl Mater* 2000, **279**: 1–18.

[19] Inaba H, Naito K, Oguma M. Heat capacity measurements of $U_{1-y}Gd_yO_2$ ($0.00 \leqslant y \leqslant 0.142$) from 310 to 1500 K. *J Nucl Mater* 1987, **149**: 341–348.

[20] Matsui T, Arita Y, Naito K. Heat capacity measurements of $U_{1-y}La_yO_2$ ($y = 0.044$, 0.090, 0.142) from 300 to 1500 K. *J Radioan Nucl Ch Ar* 1990, **143**: 149–156.

[21] Matsui T, Kawase T, Naito K. Heat capacities and electrical conductivities of $(U_{1-y}Eu_y)O_2$ ($y = 0.044$ and 0.090) from 300 to 1500 K. *J Nucl Mater* 1992, **186**: 254–258.

[22] Mills KC, Ponsford FH, Richardson MJ, *et al*. Heat capacity and enthalpy of UO_2 and gadolinia-doped UO_2. *Thermochim Acta* 1989, **139**: 107–120.

[23] Arita Y, Matsui T, Hamada S. High temperature heat capacities of $(U_{0.91}M_{0.09})O_2$ (where M is Pr, Ce, Zr) from 290 to 1410 K. *Thermochim Acta* 1995, **253**: 1–9.

[24] Arita Y, Hamada H, Matsui T. High-temperature heat capacities and electrical conductivities of UO_2 doped with simulated fission products for 2–10 at% burnup. *Thermochim Acta* 1994, **247**: 225–236.

[25] Inaba H, Naito K, Oguma M, *et al*. Heat capacity measurement of gadalonia doped (7.3 mol%) UO_2 from 310–1370 K. *J Nucl Mater* 1986, **137**: 176–178.